SYNTHETIC APERTURE IMAGING WITH SONAR AND RADAR: A COMPARISON

H.D. Griffiths
University College London, Department of Electronic and Electrical Engineering,
London, UK
h.griffiths@ee.ucl.ac.uk

Abstract

A significant number of high resolution synthetic aperture sonar systems are now being developed and evaluated. The paper presents a brief introduction and discussion of the principles of synthetic aperture imaging, then presents a comparison between the techniques, technologies and applications of synthetic aperture radar and synthetic aperture sonar, including synthetic aperture processing, motion compensation, interferometry, texture modelling and target recognition. A number of areas are suggested in which further cross-fertilization between the two domains might be fruitful: in particular, the application of differential interferometry to SAS might be investigated, and that some of the image superresolution and target recognition algorithms developed for high-resolution airborne SAR should be evaluated with SAS images and targets. Roll angle estimation and correction algorithms developed for aircraft-borne SAR could also usefully be evaluated with interferometric SAS data.

Introduction

The techniques of aperture synthesis have their origins in radioastronomy [1], and Ryle and Hewish were awarded the Nobel Prize for Physics for their work in this field. At much the same time (the early 1950s) it had also been realized that the cross-range resolution of a sideways-looking airborne radar (SLAR) could be improved by filtering (a technique known as *Doppler beam-sharpening*) [2]. These ideas were pursued and developed at the University of Illinois [3], and at the Willow Run Laboratory of the University of Michigan (the forerunner of the Environmental Research Institute of Michigan - *ERIM* - one of the leading US laboratories in the field of SAR).

In those days, since digital computers were in their infancy, the processing had to be done by optical means, recording each echo as a line on a strip of film, and illuminating the film (once developed) by an expanded laser beam, obtaining the image in the image plane of a Fresnel lens [4].

In the decades that followed, great advances were made in all aspects of SAR techniques and technology, with applications both in military surveillance and in geophysical remote sensing. The first satellite-borne SAR was carried by NASA's SEASAT mission in 1978. This operated for only three months, till a power failure caused a premature end to the mission, but in that time the SEASAT SAR had provided a wealth of imagery from oceans, land and ice surfaces, which emphatically demonstrated the potential of spaceborne SAR.

In the early 1960s it had been realized that such techniques might also be applied to underwater acoustic imaging [5, 6, 7]. It had originally been supposed that the instability of the underwater medium would preclude this, but measurements showed that propagation might be sufficiently stable [8]. Work on SAS has followed, principally for short-range high-resolution applications in mine countermeasures, and is now starting to yield the first practical systems.

Whilst it is evident that SAR and SAS have much in common, cross-fertilization between the two domains has been limited. The purpose of this paper is therefore to present a comparison between the techniques, technologies and applications of synthetic aperture radar and synthetic aperture sonar.

Theory of Synthetic Aperture Imaging

This section presents a brief review of the principles of synthetic aperture imaging, including a derivation of the achievable azimuth resolution and of the constraints on maximum unambiguous range.

Azimuth Resolution

The basic theory of synthetic aperture imaging with an active sensor considers the variation in pathlength from the sensor, moving along a straight line trajectory, to a point target (Figure 1).

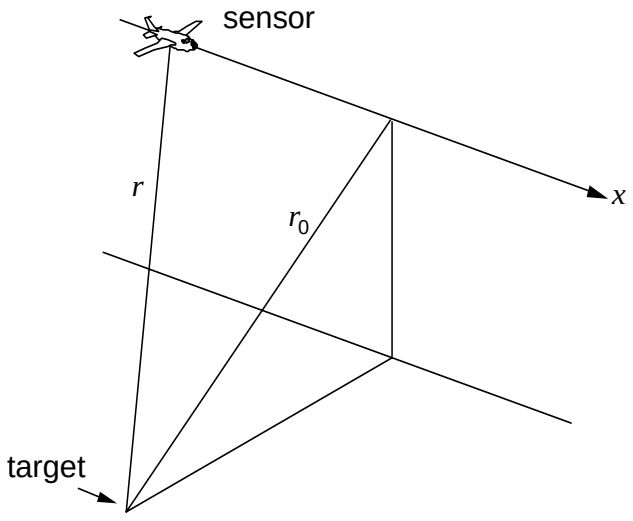

Figure 1. Geometry of synthetic aperture .

To first order the range $r(x)$ from the sensor to the target is given by:

$$r = r_0 + \frac{x^2}{2r_0} \tag{1}$$

where r_0 is the minimum value of r and x is the position of the sensor along its path such that $x = 0$ when $r = r_0$.

This can also be considered in terms of the Doppler history of the sequence of echoes from the target, which is the rate of change of the two-way range:

$$f_D = -\frac{2v}{r_0\lambda}x \tag{2}$$

where v is the sensor velocity and λ is the wavelength. This represents a linear variation of f_D as a function of x, in a similar manner to the variation of frequency of a linear FM chirped pulse (Figure 2). In an analogous manner to the matched filtering of a chirped pulse in pulse compression, synthetic aperture processing consists of matched filtering of the variation of Doppler shift along the synthetic aperture.

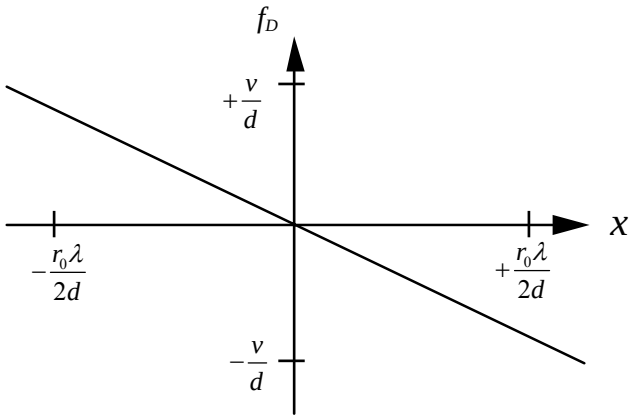

Figure 2. Doppler history of echoes from a point target. The synthetic aperture process is one of matched filtering of this Doppler history.

The time T taken to form the synthetic aperture corresponds to the time for which the target is within the footprint $r\lambda/d$ of the transducer, where λ is the signal wavelength and d is the along-track transducer dimension, thus:

$$T = \frac{r_0\lambda}{vd} \tag{3}$$

so that

$$\frac{1}{T} = \frac{vd}{r_0\lambda} \tag{4}$$

and the target extent Δx which corresponds to a Doppler resolution of $1/T$ is therefore:

$$\Delta x = \frac{r_0\lambda}{2v}.\frac{vd}{r_0\lambda} = \frac{d}{2} \tag{5}$$

giving the basic result that the azimuth resolution of a stripmap mode synthetic aperture system is equal to half the along-track transducer dimension.

Better resolution than this can be obtained by spotlight mode operation, in which the transducer beam is steered dynamically as the sensor moves along its path, to point at a given target scene for a longer time, thereby allowing a longer synthetic aperture to be formed with consequent higher azimuth resolution. The resolution achieved in this way depends on the change in aspect angle $\Delta\theta$ of the target:

$$\Delta x = \frac{\lambda}{4\sin(\Delta\theta/2)} \tag{6}$$

For a fixed beam ($\Delta\theta = \lambda/d$) this reduces to the result of equation (5), as would be expected.

Range and Azimuth Ambiguities

The Doppler shift (2) must be sampled at a sufficient rate to avoid the effects of aliasing. This implies that the sample rate (the pulse repetition frequency) must satisfy:

$$PRF > \frac{2v}{d} \tag{7}$$

In practice, because of the finite sidelobe level of the along-track transducer, the PRF may need to be greater than this minimum value.

Associated with the PRF is a maximum unambiguous range:

$$r_{\max} = \frac{c}{2.PRF} \tag{8}$$

where c is the velocity of propagation.

Equations (7) and (8) together provide a constraint on the maximum unambiguous range, for a given azimuth resolution and platform velocity [9].

The constraint is generally not a problem for aircraft-borne SARs, but limits the swath width for satellite-borne SAR systems to typically 100 km. So-called ScanSAR techniques may be used to increase

this, using an electronically-scanned antenna in the elevation plane. For high-frequency SAS systems, however, the constraint is very severe, and a number of techniques, including multiple orthogonally-coded waveforms, multiple beams, and multi-element along-track arrays, have been investigated to attempt to overcome the problem. The latter seems to be the most suitable approach, since multi-element arrays can also be used to address the problem of motion compensation in SAS systems, as well as permitting spotlight and squint mode operation.

Synthetic aperture processing

The processing to obtain the synthetic aperture image is essentially one of two-dimensional matched filtering, firstly to compress the received echo from each pulse, and then to form the synthetic aperture by matched filtering the variation of phase (or equivalently, Doppler) across the synthetic aperture, as indicated in equation (2). The various synthetic aperture processing algorithms that have been devised are essentially efficient ways of performing this matched filtering, taking into account the 'range migration' effects that occur when the range excursion at the edge of the synthetic aperture is greater than the range resolution. Among the best-known of these are the polar format algorithm [10], the chirp scaling algorithm [11] and the range-Doppler algorithm [12].

An efficient synthetic aperture processing algorithm – the Fast Factorised Backprojection algorithm – was developed by workers at FOA in Sweden to process data from an ultra-wideband aircraft-borne SAR system, operating at VHF frequencies, and used for foliage penetration applications to detect vehicles and other targets hidden in forests [13]. This algorithm works by sequentially processing blocks of data at resolutions of successive powers of two, and provides a way of trading computational load against image resolution in a particularly efficient way.

The algorithm has also been applied to processing of SAS images [14, 15] and has been shown to exhibit the same advantages. Figure 3 shows the essential principle.

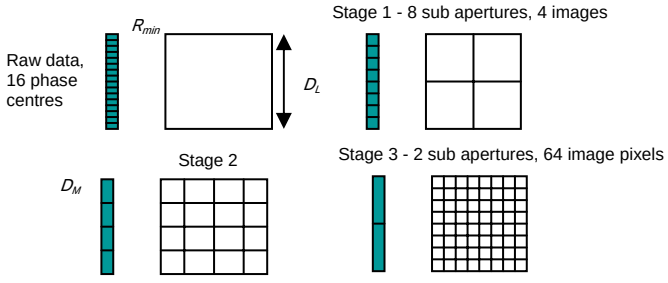

Figure 3. Principle of Fast Factorised Back Projection algorithm([14]).

Motion compensation

Compensation for motion irregularities of the sensor along its path is critical in both airborne SAR and in SAS systems (though not with satellite SAR). In the SAR domain, motion compensation algorithms have been devised based on deriving the correct matched filter for the synthetic aperture processing, by contrast optimization, multilook registration, or phase gradient techniques [16]. The problem is particularly acute for SAS systems, as opposed to SAR, because the underwater platform moves relatively slowly and some tens of seconds may be needed to form the synthetic aperture. However, with SAS it is much more usual to employ an along-track receive array with multiple receiver channels. This allows correlation-based micronavigation algorithms to be used.

An important parameter of motion compensation of both Inertial Navigation Systems (INS) and autofocus algorithms is their frequency response, in other words their ability to respond to motion errors of a given spatial frequency. Another important factor is the texture of the seabed to which they are applied.

With SAS systems, variants of the DPCA (Displaced Phase Centre Array) algorithm have been found to perform well, especially when augmented with INS data and followed with other autofocus algorithms (such as the phase gradient algorithm (PGA)) in cascade [17, 18].

The DPCA algorithm relies on ping to ping correlation of individual hydrophone elements, and can provide a measure of both sway and yaw of the sonar array The stages in its operation may be summarized as follows:

(1) Cross-correlate the response measured at selected phase centres of ping *n* with several nearby phase centres of ping (*n*+1). The magnitude of the correlation peak is greatest when the two phase centres are closest. The along-track displacement is estimated and subsequently integrated over all pings to yield the actual surge of the platform.
(2) The lag of the correlation peak together with the phase of the correlation function gives an accurate measure of across-track motion between the two pings.
(3) Two correlated pairs of phase centres separated by distance *D*/2 are used to estimate the lateral drift and the local rotation of the array associated with each temporal analysis window

The stages in the operation of the PGA algorithm may be summarised as follows:

(1) The range-compressed sonar data are 'dechirped' by multiplication in azimuth with the appropriate matched filter.

(2) The azimuth Fourier transform is taken, transforming along-track distance into wavenumber k_u. The result is a blurred image of the seabed in which each point is convolved with the Fourier transform of the phase error.
(3) The strongest scatterer in each range line is identified, shifted to the origin, and a suitable window is applied to exclude other contributions.
(4) Inverse Fourier transform of the windowed data yields an estimate of the phase error. A maximum-likelihood estimate of phase error across the whole image is obtained by suitably combining the windowed range lines.

This cascaded scheme has been shown to be capable of excellent results, with well-focused high-resolution spotlight and squint mode images at ranges well in excess of 250 m [17, 18].

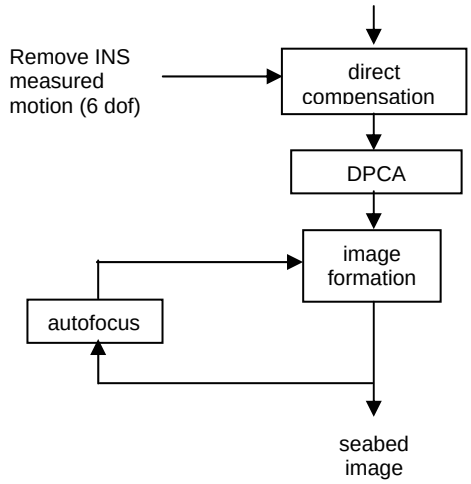

Figure 4. Three-stage motion compensation scheme used for SAS imagery.

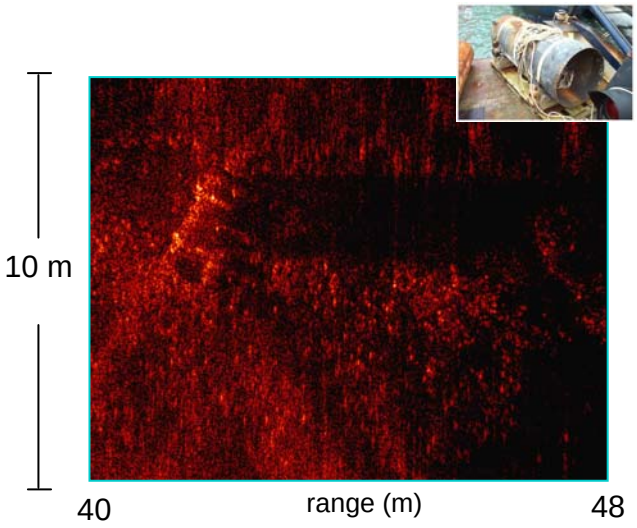

Figure 5. Strip-map image from UUV-mounted SAS system of cylindrical target (upper right) at a range of 40 m, using motion compensation scheme of Figure 4, though without INS.

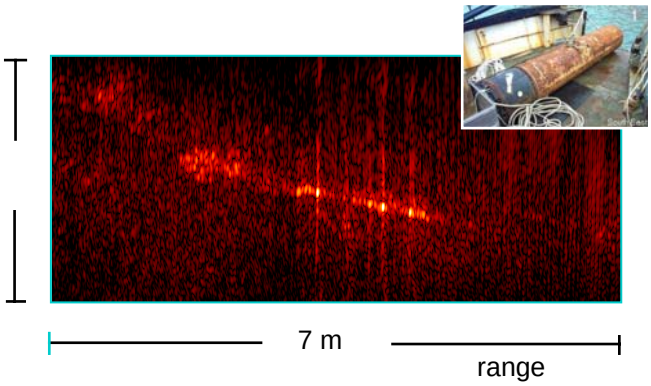

Figure 6. Spotlight-mode image from UUV-mounted SAS system, of cylindrical target (upper right) at a range of 262 m, using three-stage motion compensation scheme of Figure 4. Range pixel = 10 mm, azimuth pixel = 30 mm.

Interferometry

The principle of interferometry appears to have developed in parallel in the radar and sonar communities: in the sonar domain as bathymetric sidescan sonar [19, 20, 21], and in the radar domain as synthetic aperture radar interferometry [22, 23]. In both cases the motivation is the ability to generate maps of surface topography, but with better and better resolution the interest has expanded to the provision of target shape information, which may be important in non-cooperative target identification.

In the radar case the distinction is drawn between dual-pass interferometry, with two passes of a single SAR sensor along slightly displaced paths, and single-pass interferometry, with a single pass of a SAR sensor with two receive antennas displaced one above the other. Satellite SAR interferometry generally uses the dual-pass technique, since a dual-antenna system is almost always impractical, and the slight displacement of successive orbits due to atmospheric drag ensures displacement of the satellite to form the interferometer. On the other hand, aircraft SAR interferometry generally uses the single-pass technique, since it is very difficult with two separate passes to guarantee an acceptably-stable interferometric baseline, and it is usually not difficult to accommodate two receive arrays on a single platform. For the same reason, interferometric SAS has always used the single-pass technique.

A key part of the processing is that of 'phase unwrapping', to convert the fringe pattern or 'interferogram' (Figure 7) to height information, since the interferometric phase is ambiguous modulo-2π. Various techniques have been developed to address this; in the form of robust phase unwrapping algorithms, and the use of multiple frequencies and/or multiple elevation-plane element spacings.

When the sensitivity of the reconstructed target height to errors in all of the system parameters (i.e. baseline, roll angle, wavelength, range, …) is evaluated, it is found that errors in roll angle are the most significant. With interferometric SAR, autofocus-type algorithms have been investigated to estimate the roll angle and correct such errors from the interferometric radar data [24], and it is suggested that these algorithms should also be evaluated with interferometric SAS.

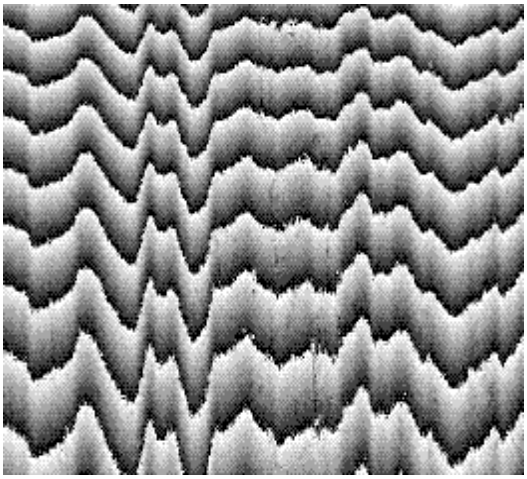

Figure 7. Interferogram (fringe pattern) from aircraft-borne interferometric SAR system [24].

Satellite SAR interferometry has been quite widely used for topographic mapping. A particularly impressive application of the technique was the X-SAR mission, in which a dual-antenna (single-pass) interferometer, using X-band and C-band frequencies, was carried by the Space Shuttle, with the second antenna mounted on a 60 m deployable boom, which represents a remarkable feat of engineering, considering the mechanical and thermal stability required. The project represented a collaboration between NASA and the German and Italian Space Agencies (DLR and ASI) , and the mission was able to provide a topographic map of approximately 80% of the Earth's land surface, between the latitudes of 60º N and 54º S, at a spatial resolution of 30 m. Such data is important for applications such as telecommunications (specifically, radio wave propagation), navigation, hydrology and disaster management.

SAR interferometry has also been used with aircraft-borne SAR systems, both to provide both land topography and (at high resolution) target shape information. In interpreting target shape information, though, it should not be expected that the targets will look like optical images, since the scattering mechanisms are different, and the effects of shadowing, layover and multipath must be taken into account.

Whilst bathymetric sidescan sonar is a well-established technique, to date, interferometric SAS has been used principally with rail-mounted systems [24, 25]. Impressive shape information from mine-like targets has been obtained by Pinto et al. [27].

Differential Interferometry

The techniques of differential interferometry were developed to measure changes in the topography of a target scene. Massonet et al. used the technique with ERS-1 SAR data to measure the displacement of the Earth's crust in the Landers area of southern California, caused by an earthquake [28]. The technique consists of subtracting two interferograms, so that any change in topography results in a set of fringes in the differential interferogram. In this example each fringe in the differential interferogram correspond to an elevation change of 28 mm, which provides an extraordinarily sensitive way of measuring elevation changes. The technique has also been used to measure changes in elevation of Antarctic ice shelves (which may provide an indication of the effects of global warming) and of volcanoes (which may provide an indication of impending eruption).

Differential interferometry does not thus far appear to have been used in SAS. It is suggested, though, that the technique may have applications in route survey, such that the appearance of new objects on the seabed (and their shape) might readily be obtained from differential SAS interferometry.

Texture modelling

Another area of common ground between SAR and SAS systems lies in the development of statistical scattering models. In the radar domain models have been developed for land and sea clutter, and in particular the Weibull and compound-K models have been widely applied [29]. The compound-K distribution represents the backscatter as the product of Rayleigh-distributed speckle:

$$f\left(x\middle|y\right)=\frac{\pi}{2y^2}\exp\left(-\frac{\pi x^2}{4y^2}\right)\quad \text{for } 0<x<\infty \tag{9}$$

and chi-distributed texture:

$$f\left(y\right)=\frac{2b}{\Gamma\left(\nu\right)}\left(by\right)^{2\nu-1}\exp\left(-b^2y^2\right)\quad \text{for } 0<y<\infty \tag{10}$$

where b is a scale parameter and ν is a shape parameter. Equations (9)and (10) are combined to yield the usual form of the K-distribution:

$$f(x) = \frac{4c}{\Gamma(\nu)}(cx)^{\nu} K_{\nu-1}(2cx) \qquad (11)$$

where $c = b\sqrt{\frac{\pi}{4}}$ is a scale parameter, ν is the same shape parameter as the chi-distributed modulation, and $K_\nu(.)$ is the modified Bessel function of the third kind of order ν. For $\nu = \infty$ the expression reduces to the Rayleigh distribution. Low values of ν (< 1) indicate 'spiky' clutter.

The compound-K distribution has also been applied very successfully to the modelling of texture in high-resolution SAR images of land scenes, and in the automatic segmentation of such images into regions of different texture [15].

Work has been done to investigate the applicability of such models to high resolution sonar images, with some success [30, 31]. As well as the basic form of the K-distribution, the modified K-distribution, in which the speckle is represented by a Ricean function, has been found to give good results.

Target recognition

Finally, in both SAR and SAS images the ultimate goal is usually the detection and classification of specific target types. This constitutes the problem of non-cooperative target recognition (NCTR). In SAR imagery these targets might be military vehicles, and it may be particularly important to distinguish such targets from civilian trucks or buses; in SAS imagery the targets of interest are usually mines.

Work with high resolution airborne SAR imagery has demonstrated the use of superresolution algorithms, giving an improvement in image resolution by a factor of perhaps two or three under optimum conditions [32], and it may be anticipated that the same techniques should work with SAS imagery.

Understanding of target signatures is very important in this respect. Use of a long spotlight mode synthetic aperture gives the possibility of a very high resolution image (provided the scattering from individual scatterers persists over the full range of aspect angle), but the same set of data can as well be used to give lower resolution images at a range of different aspect angles. Shadow information will also provide information on target shape, and may be particularly useful in the multi-aspect images – indeed, the shadow must be regarded as an integral part of the target signature. Bell and her co-workers [33] have investigated the use of 'statistical snakes' to identify and analyze shadow regions, and the same techniques are now also being applied to target identification in SAR imagery [34].

In the case of radar targets, polarimetric information can also be used in target identification, particularly since right-angled (dihedral or trihedral) features of man-made targets exhibit characteristic polarimetric scattering behaviour. However, polarimetry is one technique that cannot translate to the sonar domain !

Conclusions

This paper has attempted to provide a comparison between the techniques of synthetic aperture radar and synthetic aperture sonar, identifying similarities and differences, where each domain may have benefited from work in the other, and perhaps where similar cross-fertilization may be beneficial in the future.

Particular similarities are that the wavelengths of microwave radar and high-frequency sonar are comparable; that many of the processing and motion compensation algorithms can be adapted from one domain to the other. Most of the differences are due to the slower (and more variable) speed of propagation of sound underwater compared to microwave signals through air, which exacerbates the motion compensation problem for SAS systems and results in a severe maximum unambiguous range limitation. However, in SAS systems multi-element along-track arrays are usable, allowing DPCA motion compensation and overcoming the maximum unambiguous range constraint, as well as allowing spotlight and squint mode operation.

In particular, it is suggested that the application of differential interferometry to SAS might be investigated, and that some of the image superresolution and target recognition algorithms developed for high-resolution airborne SAR should be evaluated with SAS images and targets. Roll angle estimation and correction algorithms developed for aircraft-borne SAR could also usefully be evaluated with interferometric SAS data.

Acknowledgements

I am grateful to all of the colleagues with whom I have worked on synthetic aperture radar and synthetic aperture sonar. I would particularly like to mention Professor Chris Baker, Dr Simon Banks, Andrea Bellettini, Professor Ralph Benjamin, Sean Chapman, Dr Jonathan Dunlop, Professor Roy Griffiths, Professor Chris Oliver, Marc Pinto, Dr Trevor Sutton, Professor Roger Voles and Dr Richard White.

I am also grateful to the organisations, including the UK Engineering and Physical Sciences Research Council, QinetiQ and its predecessors, and Thales Underwater Systems, who have supported the various pieces of work whose results are presented here.

References

[1] Ryle, M., 'A new interferometer and its application to the observation of weak radio stars', *Proc. Roy. Soc. A.*, Vol. 211, pp351-375, March 1952.

[2] Wiley, C.A., 'Pulse Doppler radar methods and apparatus', US Patent No. 3,196,436, 1954.

[3] Wiley, C.A., 'Synthetic Aperture Radars - a paradigm for technology evolution', *IEEE Trans. Aerospace & Electronic Systems*, Vol. AES-21, pp440-443, 1985.

[4] Harger, R.O., *Synthetic Aperture Radar Systems*, Academic Press, 1970.

[5] Cutrona, L.J., 'Comparison of sonar system performance achievable using synthetic-aperture techniques with the performance achievable by more conventional means', *J. Acoust. Soc. Am.*, Vol.58, No.2, pp336-348, August 1975.

[6] Williams, R., 'Creating an acoustic synthetic aperture in the ocean', *J. Acoust. Soc. Am.*, Vol.60, No.1, pp60-73, July 1976.

[7] Lee, H.E., 'Extension of synthetic aperture radar (SAR) technique to undersea applications', *IEEE J. Ocean Eng.*, Vol.4, No.2, pp60-63, April 1979.

[8] Christoff, J., Loggins, C. and Pipkin, E., 'Measurement of the temporal phase stability of the medium', *J. Acoust. Soc. Am.*, Vol.71., No.6, pp1606-1607, June 1982.

[9] Li, F.K. and Johnson, W.T.K., 'Ambiguities in spaceborne synthetic aperture radar system', *IEEE Trans. Aerospace and Electronic Systems*, Vol. AES-19, No. 3, pp389-395, 1983.

[10] Carrara, W.G., Goodman, R.S. and Majewski, R.M., *Spotlight Synthetic Aperture Radar: Signal Processing Algorithms*, Artech House, 1995.

[11] Raney, R.K., Runge, H., Bamler, R., Cumming, I.G. and Wong, F.H., 'Precision SAR processing using chirp scaling', *IEEE Trans. Geoscience and Remote Sensing*, Vol.32, No.4, pp786-799, July 1994.

[12] Bamler, R., 'A comparison of range-Doppler and wavenumber domain SAR focusing algorithms', *IEEE Trans. Geoscience and Remote Sensing*, Vol.30, pp706-713, July 1992.

[13] Ulander, L., Hellsten, H. and Stenstrom, G., 'Synthetic aperture radar processing using fast factorised back projection' Proc. *EUSAR 2000* conference, Munich, Germany, pp753-756, 23-25 May 2000.

[14] Banks, S. and Griffiths, H.D., 'The use of Fast Factorised Back-Projection for synthetic aperture sonar imaging', *Proc. Inst. Acoustics*, Vol.24, No.2, March 2002.

[15] Hunter, A.J., Hayes, M. and Gough, P.M., 'A comparison of Fast Factorised Back-Projection and wavenumber algorithms for SAS reconstruction', Proc. 5th World Congress on Ultrasonics *WCU 2003*, Paris, 7-10 September 2003.

[16] Oliver, C.J. and Quegan, S., *Understanding Synthetic Aperture Radar Images*, Artech House, 1998.

[17] Sutton, T.J., Griffiths, H.D., Hetet, A., Perrot, Y. and Chapman, S.A., 'Experimental validation of algorithms for high-resolution imaging of the seabed using synthetic aperture sonar', *IEE Proc. Radar, Sonar and Navigation*, Vol.150, No.2, pp78–83, April 2003.

[18] Sutton, T.J., Griffiths, H.D., Chapman, S.A., Crook, R. and Way, M., 'Optimizing a three-stage autofocus system for synthetic aperture imaging using a UUV', (to be presented at IEEE *OCEANS'03* Conference, San Diego, 22–23 September 2003).

[19] Denbigh, P.N., 'Stereoscopic visualization and contour mapping of the sea bed using a bathymetric sidescan sonar (BASS)', *Radio and Electron. Eng.*, Vol.53, No.7/8, pp301–307, 1983.

[20] De Moustier, C., 'The state of art in swath bathymetry survey systems', *Int. Hydrographic Rev.*, No.65, pp25-54, 1988.

[21] Denbigh, P.N., 'Swath bathymetry: principles of operation and an analysis of errors', *IEEE J. Ocean. Eng.*, Vol.14, No.4, pp289-298, October 1989.

[22] Graham, L.C., 'Synthetic interferometric radar for topographic mapping', *Proc. IEEE*, Vol.62, No.6, pp763-768, 1974.

[23] Griffiths, H.D., 'Interferometric Synthetic Aperture Radar'; *Electronics and Communication Engineering Journal*, Vol.7, No.6, pp247–256, December 1995.

[24] Bullock, R., Voles, R., Currie, A., Griffiths, H.D. and Brennan, P.V., 'Two-look method for correction of roll errors in aircraft-borne interferometric SAR'; *Electronics Letters*, Vol.33, No.18, pp1581–1583, August 1997.

[25] Griffiths, H.D., Rafik, T.A., Meng, Z., Cowan, C.F.N., Shafeeu, H. and Anthony, D.K., 'Interferometric synthetic aperture sonar for high-resolution 3-D mapping of the seabed'; *IEE Proc. Radar, Sonar and Navigation*, Vol.144, No.2, pp96–103, April 1997.

[26] Bonifant, W.W. Jr., Richards, M.A. and McClellan, J.H., 'Interferometric height estimation of the seafloor via synthetic aperture sonar in the presence of motion errors', , *IEE Proc. Radar, Sonar and Navigation*, Vol.147, No.6, pp322–330, December 2000.

[27] Pinto, M.A., Hollett, R.D., Bellettini, A. and Chapman, S.A., 'Bathymetric imaging with wideband interferometric synthetic aperture sonar', accepted for publication in *IEEE J. Oceanic Engineering*.

[28] Massonet, D., Rossi, M., Carmona, C., Adragna, F., Peltzer, G., Feigl, K. and Rabaute, T., 'The displacement field of the Landers earthquake mapped by radar interferometry', *Nature*, Vol.364, pp138-142, 8 July 1993.

[29] Griffiths, H.D., Fassi, C., Dunsmore, M., Ablett, S. and Walbridge, M., 'Statistical analysis of high resolution land clutter', Proc. *NATO Symposium on Low Grazing Angle Clutter: its Characterisation, Measurement and Application*, Columbia, MD, USA, 25–27 April 2000; RTO-MP-60, AC/323(SET)TP/12, pp25.1 – 25.10, October 2000.

[30] Griffiths, H.D., Dunlop, J. and Voles, R., 'Texture analysis of sidescan sonar imagery using statistical scattering models'; *Proc. NATO Conference on High Frequency Acoustics in Shallow Water*, Lerici, Italy; SACLANTCEN Conference Proceedings CP-45 (N.G. Pace, E. Poulinquen, O. Bergem and A.P. Lyons eds), pp187–194, 30 June – 4 July 1997.

[31] Di Bisceglie, M., Galdi, C. and Griffiths, H.D., 'Statistical scattering model for high resolution sonar images: characterisation and parameter estimation'; *IEE Proc. Radar, Sonar and Navigation*, Vol.146, No.5, pp264–272, October 1999.

[32] Special issue of *The Lincoln Laboratory Journal* on Superresolution, Vol. 10, No.2, 1997.

[33] Reed, S., Petillot, Y. and Bell, J.M., 'An automated approach to the classification of mine-like objects', to appear in *IEE Proc. Radar, Sonar and Navigation.*

[34] Bennett, A.J. and Blacknell, D., 'The extraction of building dimensions from high-resolution SAR imagery', Proc. International Conference *RADAR 2003*, Adelaide, Australia, pp182–187, 3–5 September 2003.